Physica D 240 (2011) 1449–1459

Contents lists available at ScienceDirect

Physica D

journal homepage: www.elsevier.com/locate/physd

Emergence and stability of vortex clusters in Bose–Einstein condensates: A bifurcation approach near the linear limit

S. Middelkamp [a], P.G. Kevrekidis [b], D.J. Frantzeskakis [c], R. Carretero-González [d,*], P. Schmelcher [a]

[a] Zentrum für Optische Quantentechnologien, Universität Hamburg, Luruper Chaussee 149, 22761 Hamburg, Germany

[b] Department of Mathematics and Statistics, University of Massachusetts, Amherst MA 01003-4515, USA

[c] Department of Physics, University of Athens, Panepistimiopolis, Zografos, Athens 157 84, Greece

[d] Nonlinear Dynamical Systems Group,[1] Computational Sciences Research Center, and Department of Mathematics and Statistics, San Diego State University, San Diego, CA 92182-7720, USA

ARTICLE INFO

Article history:
Received 9 December 2010
Received in revised form
20 April 2011
Accepted 1 June 2011
Available online 13 June 2011
Communicated by S. Kai

Keywords:
Bose–Einstein condensates
Vortices
Dark solitons
Bifurcations

ABSTRACT

We study the existence and stability properties of clusters of alternating charge vortices in repulsive Bose–Einstein condensates. It is illustrated that such states emerge from cascades of symmetry-breaking bifurcations that can be analytically tracked near the linear limit of the system via weakly nonlinear few-mode expansions. We present the resulting states that emerge near the first few eigenvalues of the linear limit, and illustrate how the nature of the bifurcations can be used to understand their stability. Rectilinear, polygonal and diagonal vortex clusters are only some of the obtained states while mixed states, consisting of dark solitons and vortex clusters, are identified as well. We also explore the evolution of unstable states and their transient dynamics exploring configurations of nearby bifurcation branches.

1. Introduction

Vortices are among the most striking characteristics of nonlinear field theories in higher-dimensional settings [1]. They constitute one of the remarkable features of superfluids, while playing also a key role in critical current densities and resistances of type-II superconductors through their transport properties, and are associated with quantum turbulence in superfluid helium [2]. Vortices appear also in a wide variety of fields, ranging from fluid dynamics [3] to atomic physics [4] and optical physics [5].

A pristine setting for the study of vortices at the mesoscale has emerged after the realization of atomic Bose–Einstein condensates (BECs). In this context, the so-called *matter-wave vortices* were experimentally observed therein [6], by using a phase-imprinting method between two hyperfine spin states of a ^{87}Rb BEC [7]. This achievement subsequently triggered extensive studies concerning vortex formation, dynamics and interactions. For instance, stirring the BECs [8] above a certain critical angular speed [9–12] led to the production of few vortices [12], and even of robust vortex lattices [13]. Vortices can also be formed in experiments by means of other techniques, such as by dragging obstacles through the BEC [14] or by the nonlinear interference of different condensate fragments [15]. Not only unit-charged, but also higher-charged vortices were observed [16] and their dynamical instabilities have been analyzed. It should be noted that vortices of different charges have also been examined in the case with attractive inter-atomic interactions, although only theoretically; see e.g. Refs. [17,18].

While a considerable volume of work has been dedicated to individual vortices and vortex lattices, arguably, vortex clusters consisting of only a few vortices have attracted less interest. The latter theme has become a focal point recently, through the experiments involving two vortex states (alias vortex dipoles) [19,20], as well as three vortex states [21]. In Ref. [19], vortex dipoles were produced by dragging a localized light beam with appropriate speed through the BEC, while in Ref. [20], they were distilled through the Kibble–Zurek mechanism [22], previously proposed and realized for vortices in Ref. [23]. For the nonlinear dynamics of the vortices in the dipoles of Ref. [20], see also the very recent analysis of Ref. [24]. In Ref. [21], different types of three vortex configurations were produced by applying an external quadrupolar magnetic field on the BEC. The principal ones among them were an aligned vortex "tripole" with a vortex of one topological charge straddling two other oppositely charged vortices, and an equilateral triangle of three same charge vortices. On the theoretical side, few vortex states have been considered

* Corresponding author.
E-mail address: carreter@sciences.sdsu.edu (R. Carretero-González).
[1] http://nlds.sdsu.edu/.

0167-2789/$ – see front matter
doi:10.1016/j.physd.2011.06.002

also in a number of works. It was shown, in particular, that vortex dipoles (consisting of a pair of vortices with opposite circulation) are fairly robust in BECs [25]. More elaborate states, such as dipoles, tripoles and quadrupoles, were considered in Refs. [26–29]. Dynamics of such few vortex states in the non-interacting and weakly interacting limits were studied in Ref. [30] (although these were restricted to three or fewer vortices), while the recent work of Ref. [31] connected the vortex dipoles to the instability of dark soliton stripes; see also the important earlier work of Ref. [32].

In this work, we present a unifying analysis of the existence and stability of vortex clusters (consisting of alternating charge vortices), by corroborating theoretical investigations and numerical computations. Our study in Section 2 will be based on the low-density limit of near-linear excitations, where we will illustrate how they emerge (bifurcate through symmetry-breaking bifurcations) from states of the two-dimensional (2D) quantum harmonic oscillator. Then, such theoretically identified states will be continued via numerical computations in Section 3 to the strongly nonlinear regime. From these continuations, we will be able to infer numerous previously undiscovered vortex cluster states, and elucidate their stability properties (as well as compare to the theoretical predictions). A key element of our work is the illustration of the generality of the scenario (and of its theoretical/analytical description) of such symmetry-breaking bifurcations in exploring the rich available set of nonlinear states that emerge in this system. Furthermore, the explored dynamics of the instabilities ensuing due to the bifurcations reveal transient dynamics that almost invariably involve the newly arising vortex cluster states. Finally, in Section 4, we will summarize our findings and present some directions for future work.

2. Model and theoretical analysis

We consider a quasi-2D (alias "disk-shaped") repulsive condensate confined in a highly anisotropic trap with frequencies ω_z and $\omega_\perp$ along the transverse and in-plane directions, respectively. In the case $\omega_\perp \ll \omega_z$ and $\mu \ll \hbar\omega_z$ (where μ is the chemical potential), and for sufficiently low temperatures, the in-plane part $u(x, y, t)$ of the macroscopic BEC wave function obeys the following (2 + 1)D Gross–Pitaevskii equation (GPE) (see, e.g., Ref. [4]):

$$i\hbar\partial_t u = \left[-\frac{\hbar^2}{2m}\nabla_\perp^2 + V(r) + g_{2D}|u|^2 - \mu\right]u, \tag{1}$$

where $\nabla_\perp^2$ is the in-plane Laplacian, while the potential is given by $V(r) = (1/2)m\omega_\perp^2 r^2$ (where m is the atomic mass). The effective 2D nonlinearity strength is given by $g_{2D} = g_{3D}/\sqrt{2\pi}a_z = 2\sqrt{2\pi}aa_z\hbar\omega_z$, with $g_{3D} = 4\pi\,\hbar^2\,a/m$, a and $a_z = \sqrt{\hbar/m\omega_z}$ denoting, respectively, the three-dimensional (3D) interaction strength, the s-wave scattering length, and the transverse harmonic oscillator length. Eq. (1) can be expressed in the following dimensionless form,

$$i\partial_t u = \left[-\frac{1}{2}\nabla^2 + V(r) + |u|^2 - \mu\right]u, \tag{2}$$

where the density $|u|^2$, length, time and energy are respectively measured in units of $(2\sqrt{2\pi}aa_z)^{-1}$, a_z, ω_z^{-1} and $\hbar\omega_z$. Finally, the harmonic potential is now given by $V(r) = (1/2)\Omega^2 r^2$, with $\Omega = \omega_\perp/\omega_z$. From here on, all equations will be presented in dimensionless units for simplicity.

Below, we will analyze the existence and linear stability of the nonlinear states of Eq. (2). Numerically, these states will be identified as a function of the chemical potential μ by means of a fixed point (Newton iteration) scheme over a rectangular 2D grid with suitably small spacing. We will also explore the linear (spectral) stability of the obtained states by means of the Bogoliubov–de Gennes (BdG) analysis. The latter involves the derivation of the BdG equations:

$$\begin{pmatrix} \mathcal{L}_1 & \mathcal{L}_2 \\ -\mathcal{L}_2^* & -\mathcal{L}_1^* \end{pmatrix}\begin{pmatrix} a(x,y) \\ b(x,y) \end{pmatrix} = \omega\begin{pmatrix} a(x,y) \\ b(x,y) \end{pmatrix} \tag{3}$$

where

$$\mathcal{L}_1 = -\mu - \frac{1}{2}\nabla^2 + V(r) + 2|u|^2$$

$$\mathcal{L}_2 = u^2,$$

which stem from the linearization of the GPE (2) around the stationary solution $u_0(x, y)$ via the ansatz

$$u = u_0(x, y) + [a(x, y)e^{i\omega t} + b^*(x, y)e^{-i\omega^* t}], \tag{4}$$

where $*$ denotes complex conjugate. The solution of the ensuing BdG eigenvalue problem (3) yields the eigenfunctions $\{a(x, y), b(x, y)\}$ and eigenfrequencies ω. Due to the Hamiltonian nature of the system, if ω is an eigenfrequency of the Bogoliubov spectrum, so are $-\omega$, ω^* and $-\omega^*$. Note that a linearly stable configuration is tantamount to $\mathrm{Im}(\omega) = 0$, i.e., all eigenfrequencies being real. It is important to mention that, in what follows, we only resolve the relevant eigenvalues up to 10^{-2} due to computational domain constraints and therefore all eigenvalues smaller than 10^{-2} will be omitted in the figures.

Within the BdG analysis, a relevant quantity to consider is the *norm* × *energy* product of a normal mode with eigenfrequency ω, namely,

$$E = \int \mathrm{d}x\mathrm{d}y(|a|^2 - |b|^2)\omega. \tag{5}$$

The sign of this quantity, known as *Krein sign* [33], is a topological property of each eigenmode. In particular, if this sign is negative and such a mode collides with a mode of positive Krein signature, then, typically, complex frequencies appear in the excitation spectrum, i.e., a dynamical instability arises [33]. We refer to this as an oscillatory instability. Furthermore, dynamical instabilities may arise due to a real mode eigenfrequency becoming imaginary. This typically coincides with a bifurcation of a new state.

In the context of Eq. (2), it is useful to consider the low-density (linear) limit. There, eigenstates of the 2D quantum harmonic oscillator have the form $u_{nm}(x, y, t) = H_n(x)H_m(y)$ (as well as linear combinations thereof), where $\mu = \Omega(n + m + 1)$ and $H_k(x) = e^{x^2}(-1)^k(d^k/dx^k)e^{-x^2}$ are the Hermite functions where n, m quantify their order (and number of nodal lines) in each direction. This produces a linear limit whose first excited state has $\mu = 2\,\Omega$ and linear eigenstates u_{10} and u_{01}. Note that one of their interesting linear combinations is $u_{10} + iu_{01}$, which creates the single-charged vortex even at this linear limit; this state exists for all higher values of μ and is shown in Fig. 1, but we will not be concerned with it further herein, as our focus will be on clusters of vortices.

Each of the above mentioned linear eigenstates, u_{10} and u_{01}, represents a "stripe", i.e., a state with a nodal line. These can be continued for higher chemical potentials μ. As μ increases, this state develops into a one-dimensional (1D) dark soliton stripe, which is an exact analytical solution of Eq. (2) in the absence of the trap [34]. However, it is well known that such a state is dynamically unstable toward decay into vortex structures [35–37]. This decay can be understood from a symmetry-breaking bifurcation point of view [31,38]. In particular, it is possible to consider a two-mode (Galerkin-type) expansion, similar to the one used in the literature of double-well potentials (see e.g. Ref. [39]) in the form:

$$u(x, y, t) = c_0(t)\phi_0(x, y) + c_1(t)\phi_1(x, y), \tag{6}$$

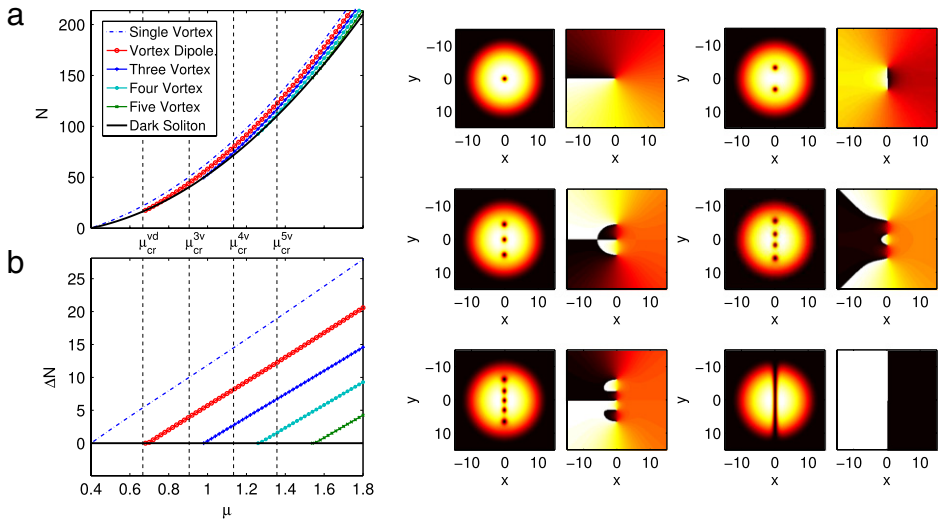

Fig. 1. (Color online) Top left panel (a): Number of atoms N as a function of the chemical potential μ for the different states for $\Omega = 0.2$ bifurcating from the dark soliton stripe. Bottom left panel (b): Corresponding atom number difference ΔN with respect to the dark soliton stripe branch. Bifurcation of vortex multipole states arises when their atom number difference from the dark soliton stripe vanishes. The corresponding theoretical predictions of such bifurcations are shown by the vertical lines. Right panels (from left to right and top to bottom): Density and phase profiles (left and right subpanels, respectively) corresponding to bifurcating states from the dark soliton stripe (bottom right panel): the single vortex state, the aligned two (vd), three (3v), four (4v) and five vortex (5v) states.

where $c_0(t)$, $c_1(t)$ are complex time-dependent prefactors, while $\phi_0 = u_{10}(x, y)$, $\phi_1(x, y) = u_{0m}$ and $m > 1$. The resulting equations and analysis are formally equivalent to the ones derived in Ref. [39] (see Eqs. (4)–(5) therein), with appropriate modifications of the inner products, but also with a *fundamental* difference. In the 1D double-well setting, only symmetry-breaking bifurcations of asymmetric real solutions are predicted (the so-called π-states that have recently been experimentally observed in Ref. [40]). The richer 2D case enables bifurcations even when the relative phase $\Delta\phi$ between the complex order parameters c_0 and c_1 is $\pi/2$. In particular, an analytical examination of the stationary version of the equations that are obtained from the two-mode reduction of Eq. (6) leads to the conclusion that such bifurcations are generically predicted at an atom number:

$$N_{\rm cr} = \frac{\omega_0 - \omega_1}{I_0 - I_1}, \tag{7}$$

where ω_0 and ω_1 are the linear state eigenvalues corresponding to ϕ_0 and ϕ_1, while $I_0 = \int \phi_0^2\phi_1^2 {\rm dxdy}$ and $I_1 = \int \phi_0^4 {\rm dxdy}$; the critical chemical potential is given by $\mu_{\rm cr} = \omega_0 + I_1 N_{\rm cr}$. In what will follow below, our analytical predictions for the bifurcation critical points will be based on the general Eq. (7), while what will change in each case are the modes ϕ_0 and ϕ_1 (and, hence, their eigenfrequencies ω_0 and ω_1, as well as the overlap integrals I_0 and I_1).

3. Numerical results and comparison with theory

The above mentioned two-mode theory provides explicit predictions for the bifurcation not only of the vortex dipole (vd) state when $m = 2$, but also for an aligned vortex tripole (3v) state (cf. the experimental observations of Ref. [21]) for $m = 3$, for an aligned vortex quadrupole (4v) state with $m = 4$, etc. In fact, there is an entire cascade of such bifurcations, as m increases, which occur progressively at $\mu_{\rm cr}^{\rm vd} = 10\ \Omega/3$, $\mu_{\rm cr}^{\rm 3v} = 86\ \Omega/19$, $\mu_{\rm cr}^{\rm 4v} = 890\ \Omega/157$, and $\mu_{\rm cr}^{\rm 5v} = 726\ \Omega/107$ for $m = 2, 3, 4, 5$ etc., respectively. Note that the number of vortices of the resulting cluster is evident by the number of intersections of the single nodal line of u_{10} with the m perpendicular nodal lines of u_{0m}, as well as the $\pi/2$ relative phase of their complex prefactors at these m intersections. Also, it is evident that the sign changing of u_{0m} at these intersections leads to an alternation of the ensuing vortex charges. Importantly, general bifurcation theory can be used to identify the stability characteristics of the resulting states. In particular, since the stripe is dynamically stable as it emerges from the linear limit, the vortex dipole state that arises from it upon the first symmetry-breaking "event" ($m = 2$) should inherit this stability. However, now, once the stripe has become unstable, all higher bifurcations with $m \geq 3$ will *necessarily* result into dynamically unstable states.

Numerical results on the symmetry-breaking bifurcations resulting in the emergence of vortex cluster states from the first excited state (single dark soliton stripe) are summarized in Fig. 1 for $\Omega = 0.2$. The emergence of $1 \times m$ ($m = 2, 3, 4, 5, \ldots$) states can be observed to occur respectively at (0.68, 0.98, 1.26, 1.54) while the corresponding theoretical predictions are $(\mu_{\rm cr}^{\rm vd}, \mu_{\rm cr}^{\rm 3v}, \mu_{\rm cr}^{\rm 4v}, \mu_{\rm cr}^{\rm 5v}) = (2/3, 0.91, 1.13, 1.36)$. Clearly, the two-mode approach captures the fundamental phenomenology, although a slight progressive degradation of the agreement on the critical point arises due to the increasing departure from the linear limit. Additionally, the linear stability properties of the resulting states directly reflect the theoretical stability expectations discussed above; see also Ref. [38].

Importantly, this approach is not restricted to the first excited state. The advantage of the bifurcation method and of the wealth of states that can be derived from it is unveiled, e.g., when considering the next set of excited states, namely the combinations with $n + m = 2$, i.e., the degenerate states u_{20}, u_{02} and u_{11}. In this setting, already a vortex *quadrupole* can be formed at the linear limit as $u_{20} + iu_{02}$ [41]. Interestingly, so can a doubly charged vortex through $u_{20} - u_{02} + 2iu_{11}$. However, these states do not present symmetry-breaking bifurcations and, therefore, are not considered further in what follows. Focusing on the states that do, some prototypical examples are (i) the solitonic state consisting of two stripes (i.e., a two dark soliton state), i.e., the u_{20} state, (ii) an X-shaped dark soliton cross emerging from $u_{20} - u_{02}$, as well as (iii) a ring dark soliton state [42] (see also Refs. [43,44]) arising from $u_{20} + u_{02}$. The u_{20} state is one for which the generalization of the phenomenology of Fig. 1 is most straightforward as with $\phi_0 = u_{20}$ and $\phi_1 = u_{0m}$ states with $2 \times m$ (2 lines of m vortices each) are formed with $m > 2$. For example, for $\phi_1 = u_{03}$ and $\phi_1 = u_{04}$, such bifurcations are predicted at $\mu_{\rm cr}^{\rm 6v2} = 283\ \Omega/67$, and $\mu_{\rm cr}^{\rm 8v2} = 2965\ \Omega/551$ (see thick black vertical dashed lines in Fig. 2), respectively, leading to $6 = 2 \times 3$ and $8 = 2 \times 4$ two-line vortex clusters. On the other hand,

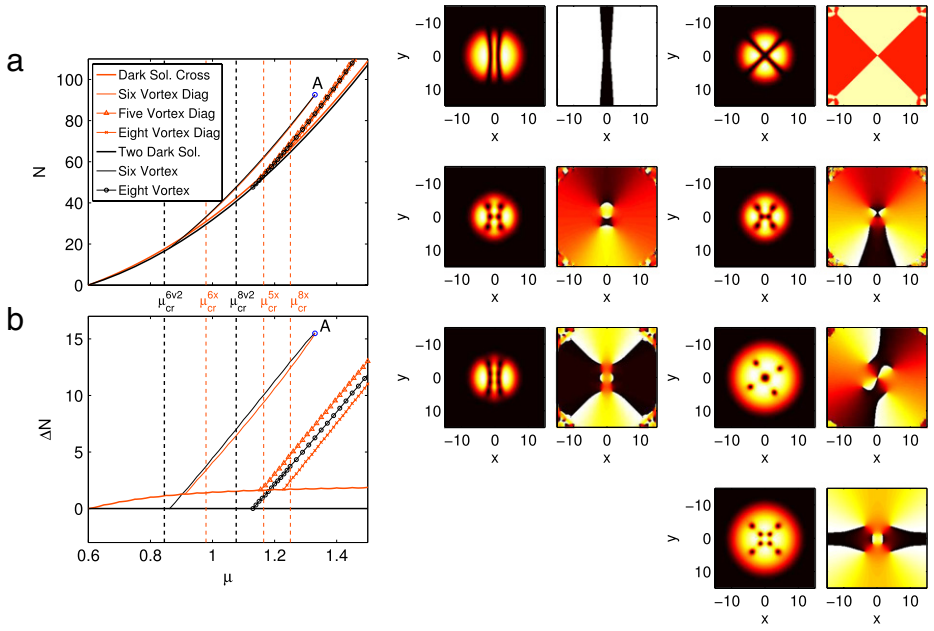

Fig. 2. (Color online) Top left panel (a): Number of atoms N as a function of the chemical potential μ for the different states bifurcating from the two dark soliton stripes (black lines) and from the dark soliton cross (orange [gray in printed version] lines) for $\Omega = 0.2$. Bottom left panel (b): Corresponding atom number difference ΔN with respect to the two dark soliton stripes branch. The occurrence of bifurcations at zero crossings of ΔN and the corresponding theoretical vertical line predictions thereof are similar to the previous (and following) figures. Middle column of panels (from top to bottom): Density and phase profiles (left and right subpanels respectively) corresponding to bifurcating states from the two dark soliton stripes (top): the aligned six (6v2) and eight vortex state (8v2). Right column of panels (from top to bottom): Density and phase profiles (left and right subpanels respectively) corresponding to bifurcating states from the X-shaped dark soliton cross (top): the diagonal six vortex state (6x), the four single and one doubly charged vortex state (5x), and the diagonal eight vortex state (8x).

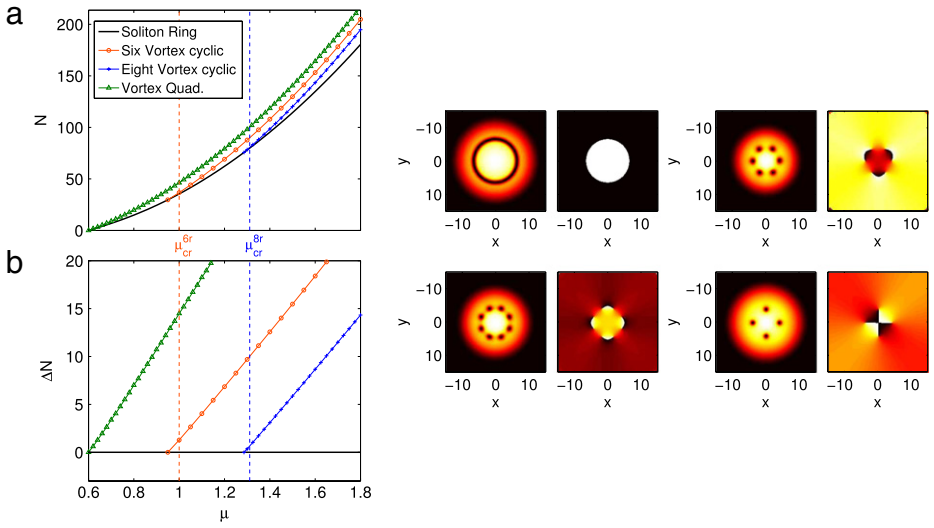

Fig. 3. (Color online) Top left panel (a): Number of atoms as a function of the chemical potential for the different states bifurcating from the ring dark soliton for $\Omega = 0.2$. Bottom left panel (b): Corresponding atom number difference with respect to the ring dark soliton. Right panels (from left to right and top to bottom): Density and phase profiles (left and right subpanels respectively) corresponding to bifurcating states from the ring dark soliton state (top left): the hexagonal (6r) and octagonal (8r) vortex states. Bottom right panel: vortex quadrupole state (note that this state does *not* bifurcate from the ring dark soliton).

the X-shaped dark soliton pair is subject to similar symmetry-breaking bifurcations/destabilizations due to $\phi_1 = u_{03}, u_{13}, u_{04}$ etc. These bifurcations, occurring in turn at $\mu_{\rm cr}^{6x} = 33\ \Omega/7$, $\mu_{\rm cr}^{5x} = 99\ \Omega/17$, and $\mu_{\rm cr}^{8x} = 369\ \Omega/59$ (see thin orange [gray in printed version] vertical dashed lines in Fig. 2), lead to a diagonal state with six vortices, a doubly charged vortex in the center together with a vortex quadrupole around it, and an eight vortex cluster of near-diagonal vortices. Finally, the ring dark soliton gets mixed with states of the form $\phi_1 = q_l(r)\sin(l\theta)$, where $q_l(r) = \sqrt{\frac{2}{2!\pi}}(r^l)\exp(-\Omega r^2/2)$, again for $l > 3$. Remarkably, these symmetry-breaking events, which can be predicted to occur, e.g., at $\mu_{\rm cr}^{6r} = 5\ \Omega$ and $\mu_{\rm cr}^{8r} = 59\ \Omega/9$ (see, respectively, orange [gray in printed version] and blue [dark in printed version] vertical dashed lines in Fig. 3), for $l = 3$ and 4, give rise to polygonal vortex configurations with the vortices now placed on the periphery of the circle. This way, vortex hexagons, octagons, decagons, etc. can be systematically constructed at will.

In Figs. 2 and 3, we explore numerically the above symmetry-breaking events for the second excited states and show besides the bifurcation diagram also typical profiles of the waveforms, as they result from varying the chemical potential. Specifically, Fig. 2 depicts the bifurcations and profiles for the states arising from the two dark soliton stripes (middle column of panels) and

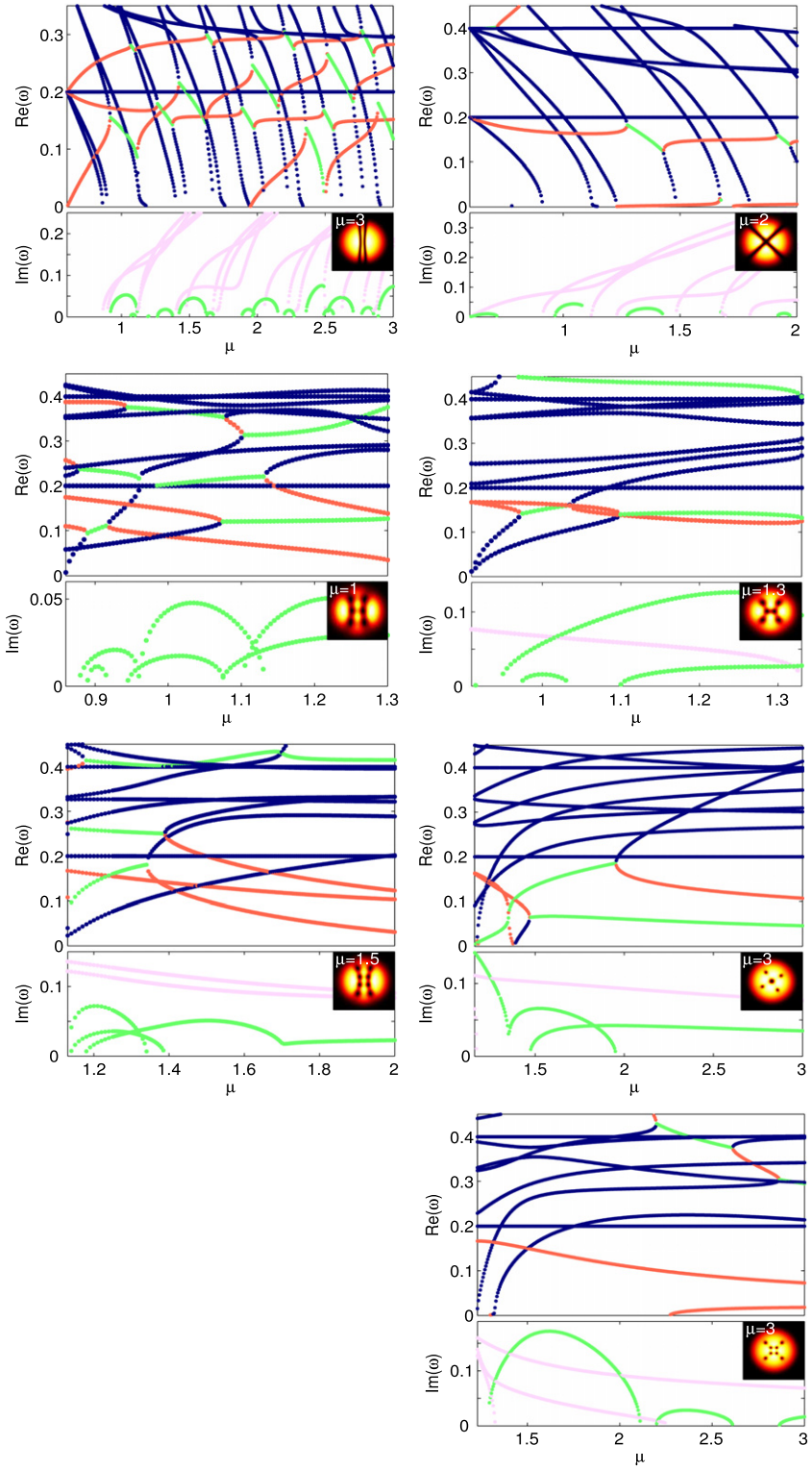

Fig. 4. (Color online) BdG spectra for the two dark soliton stripe and its bifurcating states (left column) and for the dark soliton cross and its bifurcating states (right column) corresponding to the states described in Fig. 2. The inset in each of the spectra depicts a typical configuration at the chemical potential indicated. In all BdG spectra we depict the real (top subpanel) and imaginary (bottom subpanel) parts of the eigenfrequencies as a function of the chemical potential μ using the following color coding for the online (respectively, in print) version: blue (black) = positive energy (Krein sign) modes, orange (dark gray) = negative energy modes, green (gray) = oscillatory unstable modes, and pink (light gray) = non-oscillatory unstable modes. The presence of non-vanishing imaginary parts is an indication of instability. Note that the only stable solutions are the two dark soliton stripe (top left panel) and its first symmetry-breaking offspring, the six vortex state (left panel of second row), which are stable only for low enough chemical potentials.

the dark soliton cross (right column of panels). From the two-stripe soliton bifurcates a six vortex (6v2) (2×3) state and an eight vortex (8v2) (2×4) state in the considered regime. From the X-shaped dark soliton cross bifurcates a diagonal six (6x) and eight vortex (8x) configurations, as well as a state with a vortex quadrupole surrounding a central doubly charged vortex (5x). We

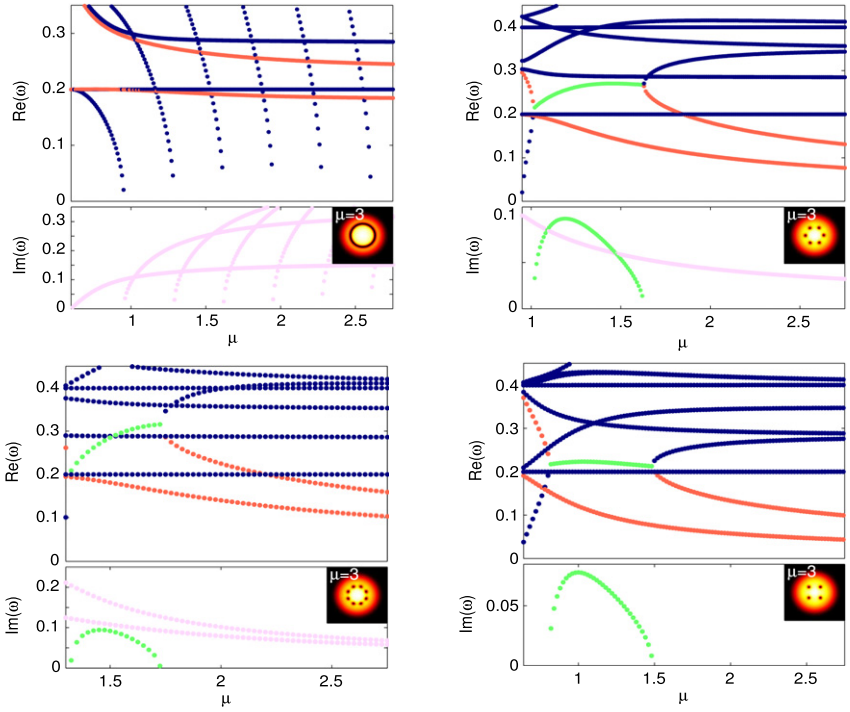

Fig. 5. (Color online) BdG spectra for the states bifurcating from the ring dark soliton and for the vortex quadrupole (bottom right) that does not itself emerge from the ring. These spectra correspond to the bifurcations depicted in Fig. 3. For an explanation of the color codes see Fig. 4. From the above it is clear that the most robust state is the vortex quadrupole (which is dynamically stable for small μ except for a narrow interval of oscillatory instabilities).

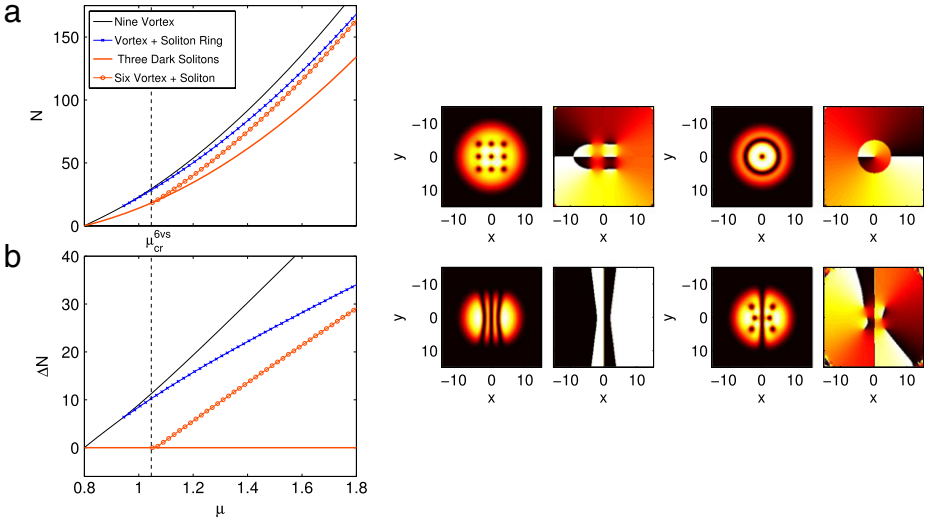

Fig. 6. (Color online) Top left panel (a): Number of atoms as a function of the chemical potential for the different states bifurcating from $\mu = 4\,\Omega$ for $\Omega = 0.2$. Bottom right panel (b): Corresponding atom difference with respect to the three soliton state. Right panels (from left to right and top to bottom): Density and phase profiles of the nine vortex state, the vortex soliton ring, the three soliton stripe state and the mixed state consisting of a dark stripe and six vortices.

also mention in passing that interesting additional bifurcation events (collisions and disappearances into "blue sky" bifurcations) arise, e.g., between the six vortex cluster deriving from the X-shaped dark soliton cross and that deriving from the two-stripe soliton (see blue circle denoted by A in Fig. 2). On the other hand, in Fig. 3 we depict the states that bifurcate from the vortex ring: vortex hexagons (6r) and octagons (8r). In this figure we also depict the vortex quadrupole state (bottom right panel) which does not bifurcate from the soliton ring. In all the cases, good quantitative agreement is found on the critical points predicted by the theory and those observed numerically.

Figs. 4 and 5 complement the above existence picture with a systematic linear stability analysis of each of the corresponding states for Figs. 2 and 3 respectively. The two-stripe soliton is dynamically stable near the linear limit, a stability inherited by its first symmetry-breaking offspring, the six vortex (2×3) state; while the aligned eight vortex case (2×4) is unstable from its existence onset (see left column of panels in Fig. 4). Similarly, the X-shaped dark soliton cross state also bears imaginary eigenfrequencies for all values of μ and hence its derivative states inherit its dynamical instability (see right column of panels in Fig. 4). On the other hand, the ring dark soliton is, as was also found earlier [41–44], always unstable, hence the polygonal vortices that derive from it inherit this instability (see Fig. 5). However, it should be noted that the instability of such states weakens as the chemical potential μ increases. Note that, the vortex quadrupole is

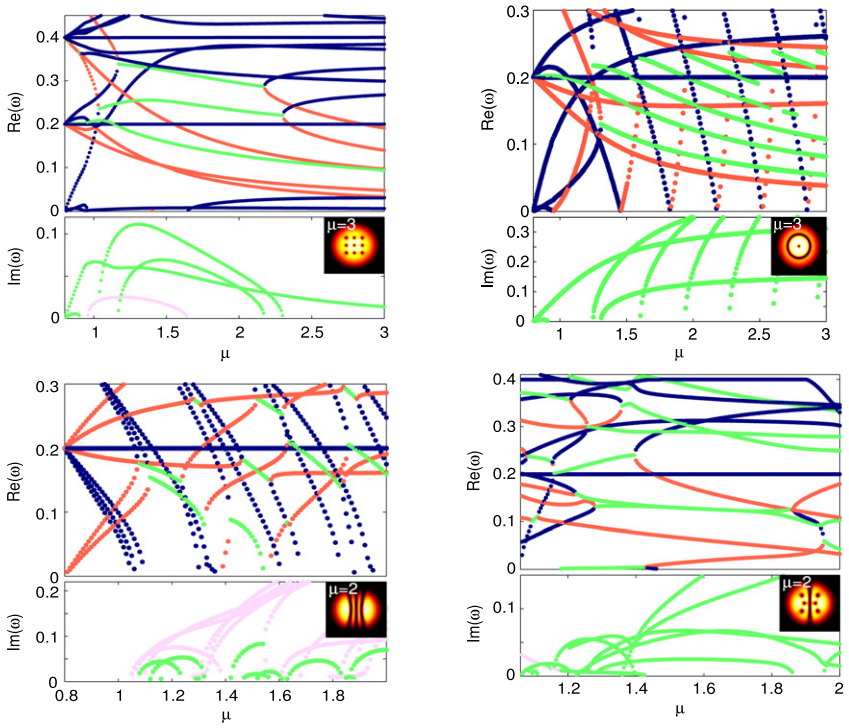

Fig. 7. (Color online) BdG spectra for the bifurcating states depicted in Fig. 6. From left to right and top to bottom: the nine vortex state, the ring dark soliton plus vortex, the three dark soliton stripe (which is stable for low values of the chemical potential), and the mixed soliton–vortex state. For an explanation of the color codes see Fig. 4.

stable in the linear limit. Since no state bifurcates from the vortex quadrupole this stability is generally preserved (apart from a small window of oscillatory instabilities).

A general comment on the observed BdG spectra is due here. We can see that the spectra bear a large number of positive Krein sign modes (see blue (black) points in all BdG spectra) which appear to be asymptoting to appropriate corresponding values in the large chemical potential limit. In addition, there is a number of negative Krein sign eigenfrequencies (see orange (dark gray) points in all BdG spectra) which may lead to oscillatory (upon collision with positive sign ones) or exponential instabilities. Generally, we can comment that the positive Krein sign eigenmodes correspond to the ground state "background" on which a particular solitonic or vortex (or mixed) state exists. Furthermore, these eigenfrequencies have a well-defined limit when μ is large as discussed e.g. in Ref. [45] (see also references therein). On the other hand, the negative Krein sign modes reflect the excited state nature of the considered soliton or vortex (or mixed) states and are the ones which bear the potential for dynamical instabilities. In the case of multi-vortex clusters consisting of individual vortices an upper bound on the maximal order of such (negative Krein) eigenstates can be given by the number of vortices in the configuration. This, in turn, also gives an upper bound on the number of potentially observable unstable eigenmodes.

Importantly, the present approach can be generalized to higher excited states. As merely a small sample of further exotic configurations that can emerge (some of which can even be structurally robust), we mention a nine vortex cluster (a square grid of 3×3 vortex "particles"), which emerges from the linear limit as $u_{30}+iu_{03}$ and can, therefore, be regarded as a higher excited analog to the single vortex and the vortex quadrupole states and is expected to be stable in the vicinity of that limit (at least with respect to purely imaginary [i.e., non-oscillatory] instabilities, see below). On the other hand, there are bifurcations from that state including the bifurcation of a ring with a vortex in its center (which was again discussed e.g., in Ref. [44]). Another state that exists and should be robust near the linear limit is a three soliton stripe. In fact, from such a state bifurcations again emerge due to the mixture with states such as $\phi_1 = u_{0m}$ with $m \geq 4$, but also with $\phi_1 = u_{1m}$ with $m \geq 3$. We focus briefly on the latter, which is theoretically predicted to occur at $\mu_{\rm cr}^{\rm 6vs} = 1250\,\Omega/239$ (see vertical dashed line in Fig. 6), because it gives rise to yet another novel type of state, namely a mixed state between vortices and a dark soliton: this soliton–vortex mixed state has a dark soliton stripe nodal line plus two additional lines over each of which three vortices reside. Similar states with eight, ten vortices etc. beside the soliton also exist, arising through subsequent bifurcations.

To corroborate the above theoretical predictions we show in Figs. 6 and 7 (again for $\Omega = 0.2$) some prototypical examples of states that emerge from the third excited linear branches and their corresponding BdG stability spectra. The nine vortex "crystal" is stable close to the linear limit in the sense that its BdG spectrum possesses no purely imaginary mode. However there is a complex mode inducing an oscillatory instability at $\mu \approx 0.95$ that vanishes again at $\mu \approx 1.6$. Close to the creation of the nine vortex crystal the vortex plus ring soliton state also bifurcates. The BdG spectrum of the vortex plus ring soliton state contains no purely imaginary mode but many complex modes. Note that the eigenvalue spectrum looks fairly similar to the ring dark soliton case, but the imaginary part of the modes is not due to imaginary modes which are created by bifurcations. In this case, modes with positive energy cross zero and thus obtain a negative energy. These negative energy modes then collide with modes with positive energy and create the complex modes. Moreover, we show the three soliton stripe, as well as the mixed soliton-six-vortex cluster state emerging from its first bifurcation event in Fig. 6. The three soliton state is stable near the linear limit (of $\mu = 0.8$) but becomes destabilized at $\mu = 1.05$ (and then further so at 1.06, 1.1 and 1.3). The first bifurcation gives rise to the very weakly unstable soliton–vortex state predicted above; the critical point for this bifurcation is found to be at $\mu = 1.034$, once again in very good agreement with the full numerical result. The present approach can naturally be extended to a multitude of additional

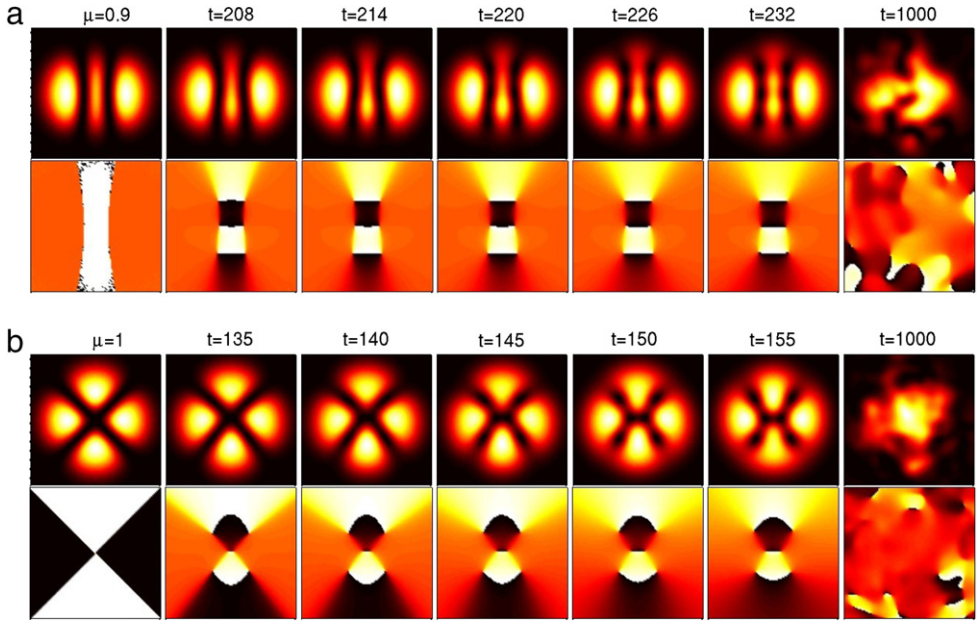

Fig. 8. (Color online) Dynamics for (a) the unstable two dark soliton stripe and (b) the dark soliton cross for $\mu = 0.9$ and $\mu = 1$ respectively. The leftmost column corresponds to the stationary steady state at $t = 0$ while the rightmost column corresponds to the configuration after a relatively long time span. The top (bottom) rows depict the condensate density (phase) at the times indicated. To initiate the instability we added to the initial steady state configuration a spatial random perturbation of magnitude 10^{-8}.

states which, however, are expected to be dynamically unstable; therefore, having presented the most fundamental ones, we will not proceed further with such considerations.

To complement the stability (i.e., stationary) picture of the bifurcating solutions we depict in Figs. 8–10 the typical destabilization dynamics for some of the modes studied above. In particular, we focus on the configurations that after an initial random destabilization evolve *temporarily* into other configurations on nearby bifurcation branches. Specifically, in Fig. 8(a) we depict the destabilization dynamics of the two dark soliton stripe where we choose a chemical potential $\mu = 0.9$ that is inside the instability window for this configuration (cf., Fig. 4). The figure shows how the two dark soliton stripe is reconfigured, through the snaking instability of its constituent two dark soliton stripes, into the six vortex state (6v2) configuration whose branch bifurcates precisely from the former stripe state at $\mu = \mu_{\rm cr}^{\rm 6v2}$ that is slightly smaller than the value $\mu = 0.9$ that we chose for this example. This reconfiguration is possible since the two branches are close to each other both in terms of the number of atoms and in terms of the actual density configuration. It is important to mention that this transient six vortex state is unstable (cf., Fig. 4) and therefore it eventually destabilizes also giving rise to a disordered state (see the last snapshot in Fig. 8(a)). A similar scenario for the dark soliton cross is depicted in Fig. 8(b) where the configuration destabilizes and transitions to the nearby configuration branch of the diagonal six vortex state (6v). Again this transient configuration is unstable and eventually destabilizes toward a disordered state. It is worth noting that the amount of vortices created in the two examples depicted in Fig. 8 depends on the length of the dark soliton stripes and the density of the background field where they are supported. This, in turn, depends of the total mass contained in the original configuration: the larger the mass (i.e., the larger the chemical potential μ) the more vortices will be nucleated by the snaking instability [46]. The dependence of the number of nucleated vortices on the mass of the underlying configuration becomes even more apparent when one studies the destabilization dynamics for the ring dark soliton, as we now discuss. Note that the dynamical evolutions below are also intimately connected with the bifurcations of Fig. 5 and the bifurcation-induced unstable modes with the largest growth rate as these are depicted for the different values of μ (considered below) within that figure. In Fig. 9 we show three examples of this destabilization for increasing mass (increasing chemical potential). For relatively low mass [panel (a) with $\mu = 1.25$] only three vortex pairs are created. While for configurations with larger mass it is possible to nucleate four vortex pairs [panel (b) with $\mu = 1.75$] or even more vortex pairs [eight vortex pairs in panel (c) with $\mu = 3.25$] arranged in a necklace configuration [42]. Again, as is the case for the soliton stripes and crosses, the ring dark soliton transiently passes through a neighboring branch configuration (a number of vortex pairs arranged in a necklace configuration) which in turn is unstable and eventually gives rise to a disordered state. It is interesting to note that for relatively large chemical potentials (cf., $\mu = 3.25$, see Fig. 9(c)) the cloud is wide enough to support a few wandering vortices. In fact, we observe that for $\mu = 3.25$ a vortex pair prevails for very long times ($t > 1000$, see last snapshot in Fig. 9(c)). The number of remaining vortices for long times depends on the annihilation of vortex pairs (vortex-anti-vortex pairs) as also observed in the dynamics of merging BEC fragments in Ref. [47]. In Fig. 9(d) we depict a few more snapshots for the vortex ring dynamics for long times where it is apparent that the initial eight vortex pairs suffer successive annihilations until $t \approx 360$ where a single vortex pair remains and survives for very long times. However, if the trap is too tight, the wandering vortices will be closer to each other and have higher chances to come into contact and annihilate (this is what happens for $\mu = 1.25$ and $\mu = 1.75$ in Fig. 9(a) and (b)). Thus, the wider the trap the longer the lifetimes will be for these wandering vortices. Finally, we depict in Fig. 10 the destabilization of a three soliton stripe and the ring soliton with a vortex state. The former transiently passes through the mixed soliton–vortex state configuration and the latter passes through the nine vortex state that eventually tends, in turn, to a disordered dynamical state. It is worth mentioning that all the configurations described above have *zero* total angular momentum except the ring soliton with a vortex state (see Fig. 10(b)). That is the reason why a single vortex remains for long times in the latter case while vortex-anti-vortex annihilations rid of all vortices in all the other cases (except, as explained above, for the soliton ring [cf., Fig. 9] for relatively large chemical potentials).

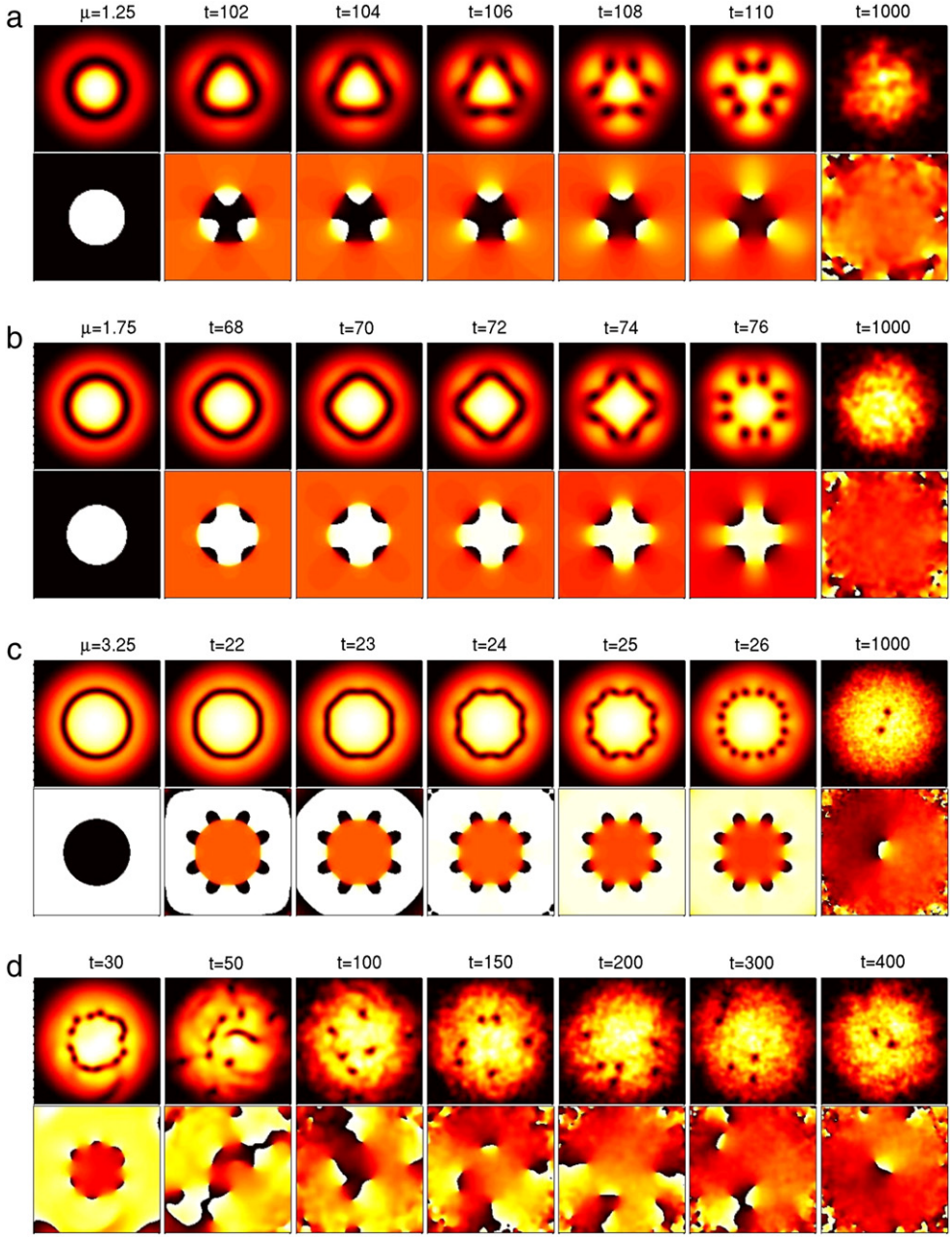

Fig. 9. (Color online) Same as in Fig. 8 for the ring dark soliton for (a) $\mu = 1.25$, (b) $\mu = 1.75$ and (c)–(d) $\mu = 3.25$.

4. Conclusions and future directions

In conclusion, in the present work we have shown that a detailed understanding of emergent vortex cluster states is possible through a near-linear-limit approach. This involves identifying the possible linear states and tracking systematically the symmetry-breaking bifurcations that can arise from them. This allowed us not only to discuss a cascade of bifurcations from the first excited state (in the form of aligned vortex clusters), but to also reveal a broad class of states emerging from the second and third excited states. These were not only rectilinear states (with "soliton-type" stripes), but also soliton rings and rings with vortices, vortex quadrupoles or nine-vortex-crystals, as well as various clusters of vortices that derive from some of these states, including vortex hexagons, octagons, decagons, $n \times m$ states (of m vortices sitting along n stripes), soliton–vortex states, and so on.

We were also able, based on the general bifurcation structure of the problem, to reveal which ones among these states are expected to be most robust, such as the vortex dipole or quadrupole, and some of the emerging vortex clusters, such as the 2×3 or the soliton–vortex state. On the other hand, nonlinear dynamics of the unstable states past the identified bifurcation points demonstrated the chiefly transient involvement of the newly arising vortex cluster states, but also, in relevant cases the above discussed robustness through the asymptotic survival of states such as the vortex dipole.

It would be especially interesting to extend this picture to different dimensions. On the one hand, one can consider the effects of anisotropy (by changing the strengths of the two different trapping directions) [48]. The examination of the novel multi-vortex cluster families presented herein and their stability is an open problem in such anisotropic settings. This should enable a "dimension-transcending" picture, as extreme anisotropies should allow to observe how the system transitions between quasi-1D and genuinely quasi-2D dynamics. On the other hand, it would

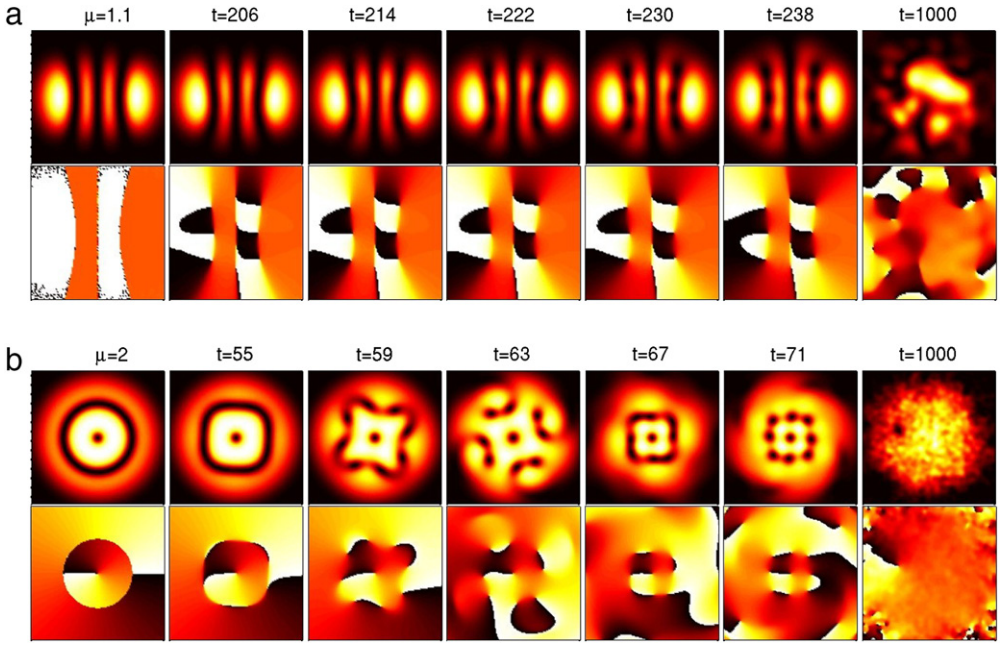

Fig. 10. (Color online) Same as in Fig. 8 for (a) the three dark soliton stripe with $\mu = 1.1$ and (b) the ring soliton with a vortex state for $\mu = 2$.

be particularly relevant and interesting to attempt to extend such considerations into 3D settings, and understand how relevant ideas generalize and how structures, such as vortex rings that have been observed in pertinent experiments[37,49], emerge. Furthermore, extensions of the present picture to the richer realm of multi-component condensates [4] would also be quite valuable. Such investigations are currently in progress.

Acknowledgments

P.G.K. gratefully acknowledges support from NSF-DMS-0349023 (CAREER), NSF-DMS-0806762 and the Alexander von Humboldt Foundation. The work of D.J.F. was partially supported by the Special Account for Research Grants of the University of Athens. R.C.G. acknowledges support from NSF-DMS-0806762. The authors also gratefully acknowledge David Hall for numerous enlightening discussions on experimental aspects of this theme.

References

[1] L.M. Pismen, Vortices in Nonlinear Fields, Oxford Science Publications, Oxford, 1999.
[2] R.J. Donnelly, Quantized Vortices in Helium II, Cambridge University Press, New York, 1991;
D.R. Tilley, J. Tilley, Superfluidity and Superconductivity, IOP Publishing, Philadelphia, 1990.
[3] A.J. Chorin, J.E. Marsden, A Mathematical Introduction to Fluid Mechanics, Springer-Verlag, New York, 1993.
[4] P.G. Kevrekidis, D.J. Frantzeskakis, R. Carretero-González, Emergent Nonlinear Phenomena in Bose–Einstein Condensates, Springer-Verlag, Berlin, 2008.
[5] A.S. Desyatnikov, Yu.S. Kivshar, L. Torner, Progress in Optics 47 (2005) 291.
[6] M.R. Matthews, B.P. Anderson, P.C. Haljan, D.S. Hall, C.E. Wieman, E.A. Cornell, Phys. Rev. Lett. 83 (1999) 2498.
[7] J.E. Williams, M.J. Holland, Nature 401 (1999) 568.
[8] K.W. Madison, F. Chevy, W. Wohlleben, J. Dalibard, Phys. Rev. Lett. 84 (2000) 806.
[9] A. Recati, F. Zambelli, S. Stringari, Phys. Rev. Lett. 86 (2001) 377.
[10] S. Sinha, Y. Castin, Phys. Rev. Lett. 87 (2001) 190402.
[11] I. Corro, R.G. Scott, A.M. Martin, Phys. Rev. A 80 (2009) 033609.
[12] K.W. Madison, F. Chevy, V. Bretin, J. Dalibard, Phys. Rev. Lett. 86 (2001) 4443.
[13] C. Raman, J.R. Abo-Shaeer, J.M. Vogels, K. Xu, W. Ketterle, Phys. Rev. Lett. 87 (2001) 210402.
[14] R. Onofrio, C. Raman, J.M. Vogels, J.R. Abo-Shaeer, A.P. Chikkatur, W. Ketterle, Phys. Rev. Lett. 85 (2000) 2228.
[15] D.R. Scherer, C.N. Weiler, T.W. Neely, B.P. Anderson, Phys. Rev. Lett. 98 (2007) 110402.
[16] A.E. Leanhardt, A. Görlitz, A.P. Chikkatur, D. Kielpinski, Y. Shin, D.E. Pritchard, W. Ketterle, Phys. Rev. Lett. 89 (2002) 190403;
Y. Shin, M. Saba, M. Vengalattore, T.A. Pasquini, C. Sanner, A.E. Leanhardt, M. Prentiss, D.E. Pritchard, W. Ketterle, Phys. Rev. Lett. 93 (2004) 160406.
[17] D. Mihalache, D. Mazilu, B.A. Malomed, F. Lederer, Phys. Rev. A 73 (2006) 043615.
[18] G. Herring, L.D. Carr, R. Carretero-González, P.G. Kevrekidis, D.J. Frantzeskakis, Phys. Rev. A 77 (2008) 023625.
[19] T.W. Neely, E.C. Samson, A.S. Bradley, M.J. Davis, B.P. Anderson, Phys. Rev. Lett. 104 (2010) 160401.
[20] D.V. Freilich, D.M. Bianchi, A.M. Kaufman, T.K. Langin, D.S. Hall, Science 329 (2010) 1182.
[21] J.A. Seman, E.A.L. Henn, M. Haque, R.F. Shiozaki, E.R.F. Ramos, M. Caracanhas, P. Castilho, C. Castelo Branco, K.M.F. Magalhães, V.S. Bagnato, Phys. Rev. A 82 (2010) 033616.
[22] T.W.B. Kibble, J. Phys. A 9 (1976) 1387;
W.H. Zurek, Nature 317 (1985) 505;
W.H. Zurek, Phys. Rep. 276 (1996) 177.
[23] C.N. Weiler, T.W. Neely, D.R. Scherer, A.S. Bradley, M.J. Davis, B.P. Anderson, Nature 455 (2008) 948.
[24] P. Kuopanportti, J.A.M. Huhtamäki, M. Möttönen, Phys. Rev. A 83 (2011) 011603(R).
[25] L.-C. Crasovan, V. Vekslerchik, V.M. Pérez-García, J.P. Torres, D. Mihalache, L. Torner, Phys. Rev. A 68 (2003) 063609.
[26] M. Möttönen, S.M.M. Virtanen, T. Isoshima, M.M. Salomaa, Phys. Rev. A 71 (2005) 033626.
[27] V. Pietilä, M. Möttönen, T. Isoshima, J.A.M. Huhtamäki, S.M.M. Virtanen, Phys. Rev. A 74 (2006) 023603.
[28] L.C. Crasovan, G. Molina-Terriza, J.P. Torres, Ll. Torner, Phys. Rev. E 66 (2002) 036612.
[29] G. Molina-Terriza, Ll. Torner, E.M. Wright, J.J. García-Ripoll, V.M. Pérez-García, Opt. Lett. 26 (2001) 1601.
[30] A. Klein, D. Jaksch, Y. Zhang, W. Bao, Phys. Rev. A 76 (2007) 043602.
[31] W. Li, M. Haque, S. Komineas, Phys. Rev. A 77 (2008) 053610.
[32] J. Brand, W.P. Reinhardt, Phys. Rev. A 65 (2002) 043612.
[33] R.S. MacKay, in: R.S. MacKay, J. Meiss (Eds.), Hamiltonian Dynamical Systems, Hilger, Bristol, 1987, p. 137.
[34] D.J. Frantzeskakis, J. Phys. A: Math. Theor. 43 (2010) 213001.
[35] E.A. Kuznetsov, S.K. Turitsyn, Zh. Eksp. Teor. Fiz. 94 (1988) 119. [Sov. Phys. JEPT 67, 1583 (1988)].
[36] D.L. Feder, M.S. Pindzola, L.A. Collins, B.I. Schneider, C.W. Clark, Phys. Rev. A 62 (2000) 053606.
[37] B.P. Anderson, P.C. Haljan, C.A. Regal, D.L. Feder, L.A. Collins, C.W. Clark, E.A. Cornell, Phys. Rev. Lett. 86 (2001) 2926.
[38] S. Middelkamp, P.G. Kevrekidis, D.J. Frantzeskakis, R. Carretero-González, P. Schmelcher, Phys. Rev. A 82 (2010) 013646.
[39] G. Theocharis, P.G. Kevrekidis, D.J. Frantzeskakis, P. Schmelcher, Phys. Rev. E 74 (2006) 056608.
[40] T. Zibold, E. Nicklas, C. Gross, M.K. Oberthaler, Phys. Rev. Lett. 105 (2010) 204101.

[41] T. Kapitula, P.G. Kevrekidis, R. Carretero-González, Physica D 233 (2007) 112.
[42] G. Theocharis, D.J. Frantzeskakis, P.G. Kevrekidis, B.A. Malomed, Yu.S. Kivshar, Phys. Rev. Lett. 90 (2003) 120403.
[43] G. Theocharis, P. Schmelcher, M.K. Oberthaler, P.G. Kevrekidis, D.J. Frantzeskakis, Phys. Rev. A 72 (2005) 023609;
L.D. Carr, C.W. Clark, Phys. Rev. A 74 (2006) 043613.
[44] G. Herring, L.D. Carr, R. Carretero-González, P.G. Kevrekidis, D.J. Frantzeskakis, Phys. Rev. A 77 (2008) 023625.
[45] P.G. Kevrekidis, D.E. Pelinovsky, Phys. Rev. A 81 (2010) 023627.
[46] Manjun Ma, R. Carretero-González, P.G. Kevrekidis, D.J. Frantzeskakis, B.A. Malomed, Phys. Rev. A 82 (2010) 023621.
[47] R. Carretero-González, B.P. Anderson, P.G. Kevrekidis, D.J. Frantzeskakis, C.N. Weiler, Phys. Rev. A 77 (2008) 033625.
[48] J. Stockhofe, S. Middelkamp, P.G. Kevrekidis, P. Schmelcher, Europhys. Lett. 93 (2011) 20008.
[49] N.S. Ginsberg, J. Brand, L.V. Hau, Phys. Rev. Lett. 94 (2005) 040403.